THE JOURNAL OF PHYSICAL CHEMISTRY C

C: Energy Conversion and Storage; Energy and Charge Transport

Novelty of Lithium Salt Solution in Sulfone and Dimethyl Carbonate-Based Electrolytes for Lithium-Ion Batteries: A Classical Molecular Dynamics Simulation Study of Optimal Ion Diffusion

Gaurav Kumar, Thejus R Kartha, and Bhabani S. Mallik

J. Phys. Chem. C, **Just Accepted Manuscript** • DOI: 10.1021/acs.jpcc.8b06581 • Publication Date (Web): 26 Oct 2018

Novelty of Lithium Salt Solution in Sulfone and Dimethyl Carbonate-based Electrolytes for Lithium-ion batteries: A Classical Molecular Dynamics Simulation Study of Optimal Ion Diffusion

Gaurav Kumar[†], Thejus R. Kartha[†], and Bhabani S. Mallik[†,*]

[†]*Department of Chemistry, Indian Institute of Technology Hyderabad, Kandi, Sangareddy-502 285, Telangana, India*

ABSTRACT: The reduction in the usage of fossil fuel can be achieved by focusing on development of high-energy storage battery. Recently, tetramethylene sulfone (TMS) based electrolytes have become the center of attraction for Li-ion battery due to its high electrochemical and thermal stability. Our work uncovers the novel effect of adding dimethyl carbonate (DMC) to the mixture of TMS with $LiPF_6$ solvent having different molar ratios of individual constituent by the classical Molecular Dynamics simulations. We calculated composite electrolyte properties such as solvation structures, diffusion coefficients, ionic conductivities and found that the coordination between Li^+ and PF_6^- is least for DMC/TMS ratio of (1:2); because Li ions are found to be more coordinated with TMS molecules, which provides better structural stability to the system. Moreover, the transport properties of this system illustrate that the diffusion of ions is not so encouraging. But, while taking different concentrations of $LiPF_6$ with the same molecular ratio of DMC/TMS, it was found that Li^+ and PF_6^- have more diffusion coefficient and ionic conductivities with the salt/solvent molar ratio of 1:20. However, due to strong interactions of Li-F, we propose a salt-solvent ratio of 1:12 as an appropriate choice based on optimal ion diffusion for better battery performance.

■ INTRODUCTION

In current scenario, alkali ion rechargeable batteries having high energy density are in great demand as energy storage sources for use in automobiles, handheld electronic machines, light electric vehicles, load leveling in electric power.[1] The electrolytes are ionic conductors which provide a medium for transfer of charge and metal ions inside the cell between negative and positive electrodes[2]. The charging and discharging processes demonstrate the efficiency of any rechargeable metal ion battery. The discharging capability of metal ion battery confides to a critical phenomenon in which metal ions and electrons can migrate through the electrolytes. The efficiency can be increased on reducing the path length over which the electrons and metal ions have to move by using nano-sized particles.[3] The electrolytes have a great significance, and can be characterized by certain basic properties. They should possess good ionic conductivity but not be electronically conductive, as this would cause internal short-circuiting. Other characteristic features are that it should not react with electrode materials, show good thermal stability and economical. Having these characteristics, electrolytes can be of different types depending on the composition of the cell: aqueous as well as non-aqueous electrolytes, ionic liquids, solid polymer electrolytes or ceramic/glassy electrolytes[4]. Aqueous electrolytes are metal ionic salts dissolved in an aqueous solvent. The main advantages of aqueous electrolytes are that they are economically viable and possess high ionic conductivity. Moreover, oxygen produced at the positive electrode diffuses through the separators and can be reduced to water at the negative electrode. This oxygen-cycle renders tolerance to overcharging, but on the other hand, the electrolytes have low decomposition voltage[5] (1.23 V). Due to their low electrochemical window, aqueous electrolytes cannot be used for high energy density rechargeable batteries. Although the problem of low electrochemical stability is somewhat resolved by eliminating oxygen by adjusting pH (10-13) value of electrolytes and by using carbon-coated electrode materials like $LiTi_2(PO_4)_3$/$LiFePO_4$, it is valid only for limited energy density metal ion batteries.[6] Recently, more advanced methods to access the aqueous regimes, namely the water-in-salt electrolytes,[7] have been proposed. These electrolytes, with higher concentrations of salt, expands the electrochemical window of water to ~3 V, which is quite interesting and opens up new avenues for further research.

Non-aqueous electrolytes are universal electrolytes for metal ion batteries as they have high electrochemical stability, high ionic conductivity and low viscosity. Non aqueous electrolytes used in commercial lithium ion battery are usually lithium hexafluorophosphate ($LiPF_6$) which is dissolved in the mixture of ethylene carbonate (EC) with dimethyl carbonate (DMC), propylene carbonate (PC), diethyl carbonate (DEC) or ethyl methyl carbonate (EMC)[8]. Organic fluoro-compounds are one of the most promising electrolyte solvents for high voltage conditions, because these compounds have higher oxidation potentials due to the strong electron-withdrawing effect of the fluorine atom.[9] Since organic solvents are mostly volatile, flammable and have a low voltage stability of conventional carbonates,[10] searching for a high-voltage, non-flammable, non-volatile and electrochemically stable electrolytes has been much important for the development of high energy density metal ion battery.[11] Sulfones are known to have high resistance to both reducing and oxidizing conditions, which provide high electrochemical stability and energy density to the systems.[12] In particular, tetramethylene sulfone (TMS) gained lots of focus due to its high oxidation potential (> 6.5V)[13], high polarity, high flash point (166 ^oC), boiling point (285 ^oC) and dielectric constant (44).[14] TMS based electrolytes were identified to have good cycling ability (1000 cycles) in a cell against high voltage

$LiNi_{0.5}Mn_{1.5}O_4$ spinel cathode.[15] However, the practical applications of these electrolytes are very limited due to high viscosity (10.34 cp at 25°C) and melting point (26°C).[16,17] Therefore, low conductivity and hindered ionic transportation of the electrolytes are observed between the electrodes. The problems of high viscosity might be reduced by addition of low melting and less viscous co-solvents. Some low melting point and less viscous organic carbonate i.e. dimethyl carbonate (DMC) having low melting point (3°C) and viscosity (0.75cp at 25°C)[17] are used to obtain the desired results, and it has been identified that mixed sulfone-carbonate based electrolytes yield excellent cathode function.[18] The advantages of using TMS are also due to its physical and chemical properties of pure and mixture with carbonates along with the formation of solid electrolyte interphase, ion diffusion and the interaction with the electrodes. Moreover, earlier studies showed that the sulfone based electrolytes have higher oxidative stability than the carbonates.[14] TMS has shown high electrochemical stability (~ 5V vs Li/Li^+).[19] Molecular simulations were also performed to investigate the effect of anion on the electrochemical stability of sulfones, and it was found that anions like BF_4^- and PF_6^- lower the oxidative decomposition of sulfones and provide more electrochemical stability[20] to the performance of battery. Therefore, in this study, we have explored the structure and dynamics of solution of $LiPF_6$ with the mixture of TMS and DMC using classical molecular dynamics simulations. Our aim is to find the electrolyte with optimal ion diffusion from the study of various mole fractions of the mixture that can be used for the better performance of lithium-ion battery.

■ COMPUTATIONAL METHODS

We applied a systematic computational approach to determine the chemical structural features and transport properties of the electrolytes that are useful for molecular level understanding of high-energy storage devices. Gromacs 5.0.4 package[21] was used for molecular dynamics simulations. For the packing of molecules in the investigated system, Packmol[22] package was used with 0.2 nm tolerance within a cubic simulation box. OPLS-AA (Optimized Potential for Liquid Simulations –All Atom)[23] force field has been used for DMC and TMS molecules. Gaussian 09 package[24] was used for initial geometry optimizations of molecules using B3LYP[25–27] method in combination with 6-311++G(d)[14] basis set. Frequency analysis was performed by the same method and basis set to confirm the optimized structure. RESP method[28] was used for fitting the charges using Antechamber module available in Amber software package.[29] Non-bonded parameters of Li^+ were taken from Lee and Rassiah's work[30] and PF_6^- non-bonded parameters were taken from S. Balasubramanian's work.[31] Forcefield parameters are provided in Tables S1 and S2 in supporting information. The adopted force fields are non-polarizable in nature. Recently, non-polarizable force field parameters were used for Li^+ cation and carbonates in a computational investigation reporting satisfactory accuracy.[32,33] The use of polarizable force fields may affect the structure and dynamics of the electrolytes, however, the systematic validation is required for components present in our simulations with various concentrations and at different temperatures. With the absence of this approach, we prefer to use the non-polarizable force fields. Long-range electrostatic interactions were managed by particle-mesh Ewald (PME) method with a cut off distance of 1.2 nm and a grid spacing of 0.1 nm**.** van der Waals interactions were handled with cut-off distance of 1.2 nm. Energy minimization to relax the strained contacts in initial configuration was performed with the steepest descent minimization algorithm. All systems were heated at 500 K for 2 ns and subsequently cooled from 500 to 330 K in 5 steps each for 2 ns to employ the temperature tolerance relationship with systems. Afterwards, isothermal-isobaric (*NpT*) equilibration was done on the annealed systems for 10 ns with 1 fs time steps at 330 K temperature and 1 bar pressure to obtain the correct density for all the systems.[34] Subsequently, isothermal-isochoric[35] (NVT) equilibration was performed for 10 ns with 1 fs time steps and finally, microcanonical ensemble[36] (NVE) simulation for 45 ns with 1 fs time step was performed to obtain the correct structural and dynamic properties of systems from the generated trajectory saved with an interval 2 ps. Trajectory Analyzer and Visualizer (TRAVIS)[37] package is used for the analysis of spatial distribution functions.

■ RESULTS AND DISCUSSIONS

Section A. Mixtures of $LiPF_6$ with various molar ratios of DMC and TMS

1. Structural properties. Initially, we performed simulations for pure (unmixed) DMC and TMS solvents with OPLS-AA force fields. After the initial *NpT* simulation, we calculated the density (Table S3) of the solvents to obtain the acceptance of the adopted force fields, and found good agreement with experimental values.[38,39] For solvation structure, first we examined the structural snapshots obtained from the MD simulations of systems, which are shown in Figure S1 (a) and (b) in the supporting information document. Here, we show CPK model of the possible nearest molecules/ions within a distance of ~ 5 Å around the Li^+ cation. We examined the systems having $LiPF_6$ in pure solvents: DMC or TMS only. We found that both the anion and DMC solvent molecules coordinated to the cation in $LiPF_6$/DMC mixture, however only TMS molecules coordinated to cation in $LiPF_6$/TMS mixture within the analyzed distance. The interaction between cation and anion is lesser in mixtures with TMS than DMC. Afterwards, we analyzed the structural snapshots (Figure 1 (a), (b) and (c)) of systems having mixed solvents with different molar ratios as well. We do not find any anion around cation in a system having DMC and TMS molar ratio of 1:2 within the analyzed distance, and we observe that on increasing the number of TMS molecules in the mixtures, the separation between cation and anion becomes more according to the earlier observation.[18] All the analysis presented till now are based on few of the instantaneous snapshots obtained from the total trajectories. To get more information about statistically averaged structural properties, we

analyzed the radial distribution functions (RDFs) and spatial distribution functions (SDFs) from the MD trajectories of NVE simulations. RDF implies the 2-dimensional probability distribution of a particle at the distance r, from a reference particle and describes the solvation structure while analyzing mixtures through simulations.[40]

We focus on the distribution of anions around the cation which was taken as reference atom in unmixed solvent and we study the pair correlation of cation with F and P atoms of the anion. Figure 2 illustrates the RDFs of anions with the reference cation in pure solvents and their corresponding number integrals. RDF of cation (Figure 2a) with phosphorous atom of anion (Li^+-P) shows larger and sharper peak in DMC than TMS, and the most probable Li^+-P distances are obtained as 3.2 and 3.4 Å with corresponding peak heights of 17.7 and 3.6 in DMC and TMS, respectively. On comparison of these RDFs with earlier studied[41] Li^+-P interaction in DMC and ethylene carbonate (EC), we find a good agreement of Li^+-P interaction in DMC and similar Li^+-P correlation in EC as well as TMS. The distribution of F atoms of anion around the cation was also calculated to get an insight into the dissociation of cation-anion pairs. We find a sharper and larger peak of Li^+-F RDF (Figure 2b) in DMC than the TMS, and the most probable Li^+-F distances are found to be 2.4 and 2.5 Å with corresponding peak heights of 14.28 and 2.65 in DMC and TMS, respectively. From the comparison of peak heights of Li^+-F, it is apparent that the ion pair separation will be more in TMS solvent than in DMC as it shows lesser interaction between Li^+-F. The lower peak heights of Li^+-P and Li^+-F RDFs in TMS show an indication of greater propensity of cation-anion separation on addition of TMS solvent. The appearance of second peak in Li^+-F RDFs in both DMC and TMS is due to the other F atoms in anion.

In addition to radial distribution functions, we also calculated the number integrals which illustrate the number density of atoms around the reference atom at distance r and is mathematically represented as:[42]

$$NI(r) = 4\pi\rho_B \int_0^{r_{NI}} (r^2 g(r))\, dr \quad \ldots\ldots\ldots (1)$$

where NI(r) represents number integral at distance r and ρ_B stands for atom density of surrounded particles. g(r) is the radial distribution function. The plateaus of number integral of Li^+-P interaction in DMC and TMS (Figure 2a) illustrate that the first solvation shell occured between 4.5 and 5.5 Å. We found number density of around 1.04 for phosphorus around the cation in DMC solvent while it was found to be 0.25 in TMS solvent. The structural snapshots corresponding to these systems are in good agreement with radial distribution functions, and the number integrals within the first solvation sphere.

After observing the structural properties of cation-anion distributions in pure solvents, we focus on mixed solvent systems. Numbers of cation, anion, and the solvent molecules comprising the systems with corresponding densities and box lengths are mentioned in Table 1. The separation of cation-anion increases on adding TMS molecules and is found to be more in the system having DMC and TMS molar ratio of 1:2. Upper panels (a and b) of Figure 3 represent the radial distribution functions of P and F atoms of anion around cation. The most probable distances of Li^+-P interaction are found about 3.2, 3.3 and 3.3 Å for 2:1(system 3), 1:1 (system 4) and 1:2 (system 5) molar ratios of DMC and TMS, respectively; the corresponding peak heights are observed at around 16.6. The number densities of anions are found to be 0.92, 0.87 and 0.82 around the cation in systems 3, 4 and 5, respectively. Another cation-anion correlation i.e. Li^+-F interaction is shown by RDF and we observe the first peak maximum at ~2.4 Å with the peak height of 12.8, 11.9 and 11.5 for systems 3, 4 and 5, respectively.

To understand the solvation of cation, we studied the RDFs of Li^+ with O_c (carbonyl oxygen atom of DMC), Figure 3c, and O_s (sulfonyl Oxygen atom of TMS), Figure 3d, of DMC and TMS, respectively. Comparing the Li^+-O interactions of pure solvents, it is apparent that cations have more interaction with oxygen atoms of DMC than TMS. This can be attributed to the greater electron density on carbonyl oxygen than the sulphonyl oxygen. The RDFs Li-O_c and Li-O_s pairs with number integrals are shown in lower panels of Figure 3. The most probable peak of Li-O_c and Li-O_s in pure solvents are observed at 2.3 Å with peak heights 33 and 19, respectively. This justifies that correlation between cations and oxygen atoms of TMS is lesser than that of DMC.

To understand the solvation of cation in mixed solvent, we calculated radial distribution functions of oxygen atoms of solvent around Li atom. (Panels c and d of Figure 3) The interaction of Li-O_c became less on addition of TMS molecules to pure DMC. However, the interaction of Li-O_s became more on adding DMC molecules in TMS. We obtain similar peak heights for Li-O_c for different molar ratio mixtures of DMC and TMS at a distance of around 2.3 Å. The plateaus of number integral of Li-O_c interaction in mixed solvent system illustrate that the first solvation shell is filled between 3 and 4 Å and the coordination numbers are about 2.70, 1.98 and 1.27 around Li^+ for system 3, 4 and 5, respectively while this value is 4.42 around Li^+ in pure DMC. However, the peak heights of Li-O_s interaction was found to be around 22.7, 22.1 and 21.6 at 2.3 Å and the number density of oxygen atoms were 2.07, 2.96 and 3.79 around Li^+ for system 3, 4 and 5, respectively. This information leads to understand that more oxygen atoms of TMS are found around the Li^+ than the oxygen atoms of DMC. To get more insight into cation-solvent interactions in mixture of solvents, we calculated the SDF as shown in Figure S2 a-c. The TMS layer of SDF atom isosurface is shown by transparent isosurface in cyan color while DMC layer is shown by lime colored opaque isosurface. The observation leads to fact that the TMS molecules are more interactive towards the cation than the DMC in the system 5 which facilitates a better solvating environment of cation by former molecules. These SDF studies are completely in agreement to the analysis of RDFs.

To get more information about salt solvation in pure and mixed solvents, we also examined the anion

solvent interaction. Figure S11 illustrates the radial distribution of oxygen atoms of DMC and TMS around the anion in the analyzed solvents. Upper plot of this figure represents the interaction of anion with O_c of DMC and lower plot represents that of the anion with O_s of TMS. The first peak maxima of PF_6^--O_c RDFs are found at ~4.3 Å with peak height 2.40, 2.02, 1.98 and 1.96 for systems 1, 3, 4 and 5, respectively. These RDFs imply that anion and DMC interaction decreases on increasing the TMS mole fraction in mixed solvent systems. The first peak maxima of PF_6^--O_s RDFs appear at ~5.18 Å with peak height 2.04, 1.93 and 1.83 for systems 3, 4 and 5, respectively. We observed a peak shift in pure TMS, which may be due to the high viscosity of TMS. But, no shift was observed for pure DMC due to different coordinating environments. With addition of DMC, height of first peak of PF_6^--O_c RDF increases, however, height of first peak of anion-O_s RDF decreases. The number integrals of corresponding RDFs illustrate that the number density of oxygen atoms of DMC is more than that observed for TMS around the anion. The panels (a) and (b) of Figure S10 illustrate the spatial distribution of DMC and TMS around the anion. Lime and cyan isosurfaces represent the number density of oxygen atoms of DMC and TMS molecules and the anion is shown by CPK model and both SDFs corrspond to an isovalue of 10.5 particles/nm^3. The complete study of interactions of solvents with cation and anion by spatial distribution functions for pure as well as mixed solvent systems are shown in Figure 4 and it is found that the cation and anion-solvent interactions are less in TMS and increase on adding DMC molecule.

Apart from these, we analyzed the clustering among the different groups present in the study to assess the number of ions remains free of aggregation with others. System 1 retains an average of 8.39 Li^+ and 7.18 PF_6^- free of agglomeration, with a cut-off distance of 4.4 Angstroms (This distance corresponds to first solvation shell in RDF of Li^+-P interactions.). This only accounts for 27.96 and 23.93 % of Li^+ and PF_6^-, respectively, and the rest remain aggregated on an average at any point of time. Such aggregations are an important factor to consider while studying electrolytic solutions, as it can have certain implications on the experimental perspective. The rest of the averages of non-aggregation are mentioned in Table S4. From the data given in the table, it is quite evident that the number of isolated Li^+ and PF_6^- ions increase with increase in composition of sulfolane. This supports the results so far exhibited by RDFs and other structural analyses.

2. Transport properties. Transport properties of the analysed systems, such as diffusion coefficient and ionic conductivity are related to movement of particles and can be calculated using MD trajectories. Mean square displacements (MSDs) of ions and solvent molecules were used to get transport properties from MD trajectories using following equation.

$$\mathrm{MSD} = \frac{1}{N}\sum_{i=1}^{N}[r_i(t) - r_i(0)]^2 \qquad \ldots\ldots\ldots (2)$$

where N is the total number of particles to be averaged, $r_i(0)$ is the reference position and $r_i(t)$ is the position at time t of the i^{th} particle. To get more accurate diffusive properties of ions, we need to calculate the diffusive motion of ions for β = 1. Mathematically, β values are defined as[43]

$$\beta(t) = \frac{d\ ln(MSD)}{d\ ln(t)} \qquad \ldots\ldots\ldots (3)$$

Einstein–Smoluchowski relation[44] was used for calculating diffusion coefficient and it is mathematically expressed as:

$$D = \lim_{t\to\infty} \frac{1}{6Nt}\sum_{j=1}^{N}[r(t) - r(0)]^2 \qquad \ldots\ldots (4)$$

In the above formula, N stands for number of particles, t stands for time, r(t) is the position of analysed ion at time t and r(0) is the reference position. MSD can also be used for computing the ionic conductivity of the system through the Nernst–Einstein relation[45] and is expressed as:

$$\sigma = \frac{N_i q^2}{V k_B T}(D^+ + D^-), \qquad \ldots\ldots\ldots (5)$$

where V is the simulation box volume, k_B is Boltzmann's constant, T is the simulation temperature in K, q is the elementary charge and D^+ and D^- are the diffusion constants of cation and anion, respectively. Initially, we calculated the mean square displacement to get diffusion coefficient of pure DMC at 298 K and plotted log(MSD) versus log(t) and β versus time and found that β values were ~1 within the simulation time of 5 to 20 ns. We obtain diffusion coefficient of 8.63×10^{-6} cm^{2}s^{-1} due to use of non-polarizable forcefields which agrees with the earlier molecular dynamics study of dimethyl carbonate by Ruggero Caminiti *et al.*[46] The experimental value of diffusion coefficient of dimethyl carbonate at 303 K was found as 26×10^{-6} cm^{2}s^{-1} by Hayamizu *et al.*[47] We also calculated the mean square displacement of TMS corresponding to β(t)=1 and found diffusion coefficient 0.89×10^{-6} cm^2/s at 330 K. The diffusion coefficient of TMS was found to be much lesser than that of DMC owing to the higher density of TMS. The corresponding MSD and β(t) plots are shown in Figure S3 of supporting information.

Figure S4 shows the diffusive motion of cation and anion for unmixed solvents. The first panel of figures represent the MSD plots versus time and second panel of figures represent log(MSD) plots versus log(t). We calculated the diffusion coefficient of cation and anion with the simulation time limit of 5 to 15 ns as the plot of log(MSD) versus log(t) show a straight line and the β(t) values show ~1 during the same simulation period. (extreme right panel of the figure). Then, considering three different systems of DMC and TMS mixtures with molar ratios 1:2, 1:1 and 2:1, calculations were done for the diffusive motion of cation and anion. The diffusive motion of cation and anion for mixed solvent systems has been shown in Figure S5. We calculated diffusion coefficients from the mean square displacement within the simulation time limits 5 to 22 ns for cation and 25 to 30 ns for anion, and we found that the cation and anion for all the systems are in diffusive regime. The values of diffusion coefficient

of cation are found to be 0.72×10^{-6}, 0.40×10^{-6}, 0.25×10^{-6} cm^2/s and as for the anion, these values are 1.06×10^{-6}, 0.47×10^{-6}, 0.29×10^{-6} cm^2/s corresponding to 3, 4 and 5 systems, respectively. The diffusion co-efficient values of cation and anion in DMC are found to be 1.45×10^{-6} and 1.94×10^{-6} cm^2/s, respectively. The diffusive motion of ionic entities in TMS is expected to be lesser as compared to DMC having the very close diffusion coefficients of cation and anion around 0.185×10^{-6} cm^2/s.

To further deepen our understanding of the transport property of cation and anion, we used the Nernst–Einstein relation to calculate the ionic conductivity of $LiPF_6$ in pure and mixed solvents. The dependencies of ionic conductivities on different molar ratio of DMC and TMS are shown in Figure 5. Low conductivity of $LiPF_6$ in unmixed TMS solvent is obviously due to high viscosity of TMS (10.34 cp at 298 K). Lithium ion batteries require high ionic conductivity for the fast transportation of Li^+ ion across the electrolyte. Ionic conductivity of $LiPF_6$ increases on adding DMC molecules and the values are observed to be at 2.04, 3.38 and 4.46 mS/cm for 0.33(System 5), 0.50(System 4), 0.66(System 3) mole fractions of DMC, respectively. The trend of ionic conductivities calculated by our MD simulation with molar fractions of DMC matches with earlier experimental ionic conductivity for the 1 M $LiPF_6$ in the TMS/DMC solvent reported by Seung-Yul Lee *et al.*[48]

Considering the correlation of ions among each other, the mutual conductivity or the correlated conductivity was also calculated as per the following equation:

$$\sigma = \frac{1}{6k_BVT}\lim_{t\to\infty}\frac{d}{dt}\langle\sum_{i=1}^{N}\sum_{j=1}^{N}[\vec{r}_i(t)-\vec{r}_i(0)].[\vec{r}_j(t)-\vec{r}_j(0)]\rangle \quad \ldots (6)$$

This equation takes into consideration all cation-cation, anion-anion and cation-anion interactions and averages those interactions over all frames of the simulation. This shows values relatively lower than that obtained from the Nernst-Einstein relation, similar to what was reported in literature.[49] These values are represented as the red line in Figure 5. Comparing both the conductivity curves, it is notable that the trend remains the same. For systems 5, 4 and 3 the correlated ionic conductivities obtained are 0.32, 0.8 and 1.32 mS/cm, respectively.

Section B. Different concentrations of $LiPF_6$ with fixed molar ratio of DMC and TMS (1:2)

We have discussed the solvation structure and transport properties of systems which have different molar ratio of DMC and TMS doped with fixed amount of $LiPF_6$ and found that the system 5 (corresponding to DMC:TMS as 1:2) may be used as one of the better stable solvents for Li-ion battery with compromise of lesser ionic conductivity. To understand the impact of concentration of $LiPF_6$ on ionic diffusion and to find a solvent with optimal ionic conductance, we set up five new systems (5 a-e) by taking different amounts of $LiPF_6$ and a constant molar ratio of DMC and TMS (1:2). We have shown details of no of chemical entitites with box length and density of corresponding systems in Table 2.

1. Structural properties. To obtain information about the solvation properties, we examined the structural snapshots of the systems within the first solvation shell after the MD simulations which are shown in Figure S6 of supporting information. In structural snapshots, we show the possible nearest molecules/ions around the Li cation in CPK model within a distance of ~5 Å. For lesser concentrated solutions, we obtained relatively weaker correlation between cation and anion i.e. there are only solvent molecules around the cation up to 1.09 M concentration and later we find more coordination of anion with cation. TMS molecules are also more attractive towards cation than the DMC molecules on increasing salt concentration. we analysed the RDFs and SDFs to get more information about structural properties. We focus on the cation-anion interaction which is shown by radial distribution functions of P and F atoms of anion around Li atom in the upper panel of Figure S12 for the various concentrations of salt in the mixture of two electrolytes. The most probable Li^+-P distance is about 3.3 Å with the corresponding peak height 27.36, 21.29, 17.36, 16.86, 16.01 and 14.02 for 0.54, 0.73, 0.90, 1.09, 1.27 and 1.45 M $LiPF_6$, respectively. The first maxima of Li^+-F RDFs are obtained ~ 2.4 Å with peak height of 18.91, 14.66, 12.06, 11.48, 11.22 and 9.87 for 0.54, 0.73, 0.90, 1.09, 1.27 and 1.45 M $LiPF_6$, respectively. These RDFs lead to inform that the cation-anion coordination is decreased on adding more number of $LiPF_6$ which are also represented by number integrals of corresponding RDFs. The plateaus of NI(r) indicates that the first solvation sphere occurs between 4.5-5.5 and 3.5-4.0 Å for for Li^+-P and Li^+-F interactions, respectively and atom densities of P and F atoms surrounded by Li atom increase on increasing the molar concentration of salt. To get more insight on cation solvation on increasing the molar concentration of $LiPF_6$, we calculated RDFs of oxygen atoms of DMC and TMS around Li atom. Initially, we focus on the Li^+-O_c RDF; the most probable distance is around 2.3 Å with the peak height of 34.43, 35.16, 32.95, 31.99, 31.46, 31.21 for 0.54, 0.72, 0.90, 1.09, 1.27, 1.45 M $LiPF_6$. These data imply that Li-O_c interaction decreases on increasing the salt concentration and show more interaction for 0.54 and 0.72 M $LiPF_6$ which are justified by the corresponding number integrals of Li-O_c RDF. The values of NI(r) found within first solvation sphere are about 1.41, 1.43, 1.33, 1.28, 1.25 and 1.22 for 0.54, 0.72, 0.90, 1.09, 1.27 and 1.45M $LiPF_6$, respectively.

The cation interaction with oxygen atoms TMS is also shown in Figure S12(d). We observe similar most probable distances(~2.3 Å) for the interaction of cation with carbonyl oxygen atom of DMC and sulfonyl oxygen atoms of TMS. The first maxima of Li-O_s RDFs are 21.29, 21.23, 21.96, 21.60, 21.00 and15.61 for 0.54, 0.72, 0.90, 1.09, 1.27 and 1.45M $LiPF_6$, respectively. These data illustrate that there is not much effect of salt concentration on Li-O_s interaction up to 1.27 M $LiPF_6$, but there is a sharp change in the peak height of Li-O_s RDF for 1.45 M $LiPF_6$ due to

appearance of more numbers of ions around the TMS molecule. This can be justified by the solvent-salt interaction that is shown by spatial distribution functions of systems in supporting information (Figure S8). Figure 6 is a representation of the changing coordination number values with respect to changing concentration of $LiPF_6$, for all the interactions where the cation is involved. Changing concentration of the electrolyte salt does not affect the distribution of different moieties around the lithium ion. The mild increase or decrease observed in this plot are due to the changing number of ions in each case. The RDFs of anion-solvent interaction for various molar concentration of salt has been shown in Figure S13. The maxima of PF_6-O_c and PF_6-O_s interactions are found at a distance around 4.5 Å. First peak height of PF_6-O_c RDF increases on adding salt ions and number integral also illustrates that the carbonyl oxygen atom density is surrounded towards Li^+ ion on increasing salt concentration. The peaks of PF_6-O_s RDFs also demonstrate that the anion-solvent correlation increases on adding salt to the system as the first peak height of PF_6-O_s interaction increases on increasing salt concentration. The second maxima of PF_6-O_s interaction is somewhat more sharp than the PF_6-O_c interaction due to the presence of two sulfonyl oxygen atoms (O_s) in TMS. Li^+ ions are more surrounded by DMC molecules than the TMS molecule in 0.54 M $LiPF_6$ salt/solvent system while the TMS molecules get more surrounded towards the cation on increasing salt concentration from 0.54 to 0.72 M.

2.Transport properties. Einstein–Smoluchowski relation was used to calculate MSD data, which were shown in left panels (a and d) of Figure S7, and then, β(t), which is the first derivative of log MSD with respect to log t, was calculated to get diffusive regime (Panels b and e). It was found that the simulation time between 5 to 13 ns for cation diffusion and 5 to 12 ns for anion diffusion show β values ~1 (Panels c and f) in various concentration of salt/solvent systems. We used this simulation time limit for the calculation of diffusion coefficient of cation and anion. We also plot log(MSD) versus log(t) within this simulation time limit and found a straight line for cation as well as anion in various systems which was also shown in panels b and e. The values of diffusion coefficients are shown in Figure 7. A high diffusion coefficient of anion is obtained for 0.52 M $LiPF_6$ and later it decreases readily on increasing salt concentration. The reason of high diffusion of ions at low concentration can be explained by the structural properties of this system: DMC and TMS molecules have more coordination towards cation than the anions. The diffusion coefficient of cation decreases on increasing the salt concentration because the distribution of cation and anion are decreased across the electrolyte which we have already discussed in structural properties of the systems. The effect of ionic conductivity on changing salt concentration has been shown in inset of Figure 7. Initially, system shows more ionic conductivity of $LiPF_6$ and then it decreases on adding salt concentration due to less diffusive motion of ions. Spatial distribution functions (Figure S8) of salt-solvents show that there is very less contribution of anion around DMC as well as TMS for the 0.52 M salt/solvent system which can justify the large value of ionic conductivity of this system than others. System with 0.54 M salt concentration shows highest ionic conductivity, but thermal stability of $LiPF_6$ may be decreased due to high Li-F interaction. System, which has 0.90 M salt concentration show higher ionic conductivity than the 0.72 M salt system and this system, also has a better thermal stability. We can propose this system to be used as a good electrolyte for the better performance of battery than other systems.

***Section C*. Effects of temperature for the optimal diffusion of ions**

To understand the effect of temperature on the structure and efficiency of the $LiPF_6$/TMS/DMC electrolyte system, simulations were carried out over a temperature range of 260-360 K with a gap of 10 K. The system with 2:1 molar ratio of TMS: DMC was chosen to conduct this study. From the RDFs calculated at various temperatures, (Figure S14) it is understood that the peak height undergoes little change with change in temperature accompanied by no difference in distances. The most probable distances for Li-P interactions was found to be at 0.33 nm with peak heights 21.88, 19.71, 17.51, 17.47, 19.71, 21.24 corresponding to 260, 280, 300, 320, 340 and 360 K, respectively. The interactions between O in TMS with Li^+ decreases with increase in temperature. A similar maximum is also observed for Li-O of DMC interactions at 2.3 Å. Also, an overlapping second maximum is observed for Li-O interactions at ~4.7 Å with respect to TMS and ~4.4 Å with respect to DMC. Figure 8 shows the changing coordination numbers with respect to change in temperature, and it is observed that these values remain almost same throughout. From this, it may be concluded that the distribution of different groups around the Li^+ ion does not undergo much changes with change in temperature, but the way they interact does undergo changes.

The panels, a and d, in Figure S9 show calculated MSD of the system at various temperatures. The related β(t) values can be seen in the panels, c and f, of the same figure. β(t) values show the diffusive regime to be 6-18 ns for both cases, with PF_6^- anion exhibiting lower β(t) values at 260, 270 and 280 K. This time period was used for calculating the diffusion coefficients. The increase in values of diffusion coefficients is observed with increase in temperature. Consequently, ionic conductivity, calculated from diffusion coefficients, also showed similar characteristics, which is represented in Figure 9. The correlated conductivity equation yields lower values for the ionic conductivity, and this is expected since this equation takes into consideration of all anion-anion, anion-cation and cation-cation interactions. Correlated ionic conductivity will have lesser values as all ions move quite slowly at low temperatures and the diffusivity of one ion depends on the motion of all the other related ions, unlike the case of Nernst-Einstein equation where only self-diffusivity of the ion is considered for ionic conductivity calculations.

The conductivity of the ions, which was calculated both by means of Nernst-Einstein relation and correlated conductivity equation is analyzed in terms of Arrhenius exponential function. The Arrhenius equation can be used to derive the activation energy of conduction for ions:

$$\sigma = \sigma_0 \exp\left(\frac{-E_a}{k_B T}\right) \ldots\ldots\ldots (7)$$

Since, this is similar to an equation of a straight line, a graph can be plotted for ln σ with respect to 1/T to obtain a straight line with slope $-E_a/k_B$. (inset panel A of Figure 9). Here, the activation energy for ionic conduction is calculated to be 5.4903 x 10^{-20} J (0.3426 eV). Previously, Hayamizu reported similar graphs for a system of $LiPF_6$ in EC/DEC mixtures.[50] There was also a report of activation energy for lithium ions to be ~0.53 eV in a thin film cathode using electron strain microscopy.[51] In this study, the activation energy corresponding to the correlated conductivity is found to be 4.5202 x 10^{-20} J (0.2821 eV). These observations may be due to the fact that the activation energies decreases systematically with decreasing viscosity of the system due to increase in temperature. We also present the degree of ionicity, the ratio of correlated conductivity and the value obtained from Nernst-Einstein relation, in the inset panel B of Figure 9. This quantity primarily provides the deviations from Nernst-Einstein relation due to formation of aggregation involving ions. The molecular and structural effect that controls the degree of ionicity usually originates from both ion-ion and ion-solvent interactions. The degree of ionicity decreases with temperature, however noticeable change in coordination number of cation-anion is not observed presumably due to presence of other solvent molecules.

■ SUMMARY AND CONCLUSIONS

We performed classical molecular dynamics simulations to investigate structural and transport properties for DMC/TMS/$LiPF_6$ systems by using different molar mixture of DMC and TMS as well as $LiPF_6$. Sulfolane has high electrochemical stability window and very high flash point than the carbonates based electrolytes but former molecule is also more viscous and less diffusive. Most of the electrodes consist of active material mixed with an electron conductor and a polymer and the volume among the particles of electrodes should be filled with electrolytes. Hence we need less viscous, more diffusive as well as more thermal stable electrolyte. Therefore, DMC was added as a co-solvent to reduce the viscosity of systems. Initially, we calculated Li-P and Li-F interactions for unmixed solvent systems and found weak interaction of Li-F in TMS, which illustrates that the salt is more stable in TMS than DMC. Analysis of cation-anion and cation-solvent interactions in mixed solvent systems indicate that Li^+ ions have more tendencies to coordinate with TMS while anions coordinate with DMC during the solvation of $LiPF_6$ in DMC and TMS solvent with the molar ratio of 1:2.

A result of diffusion coefficient of ions in the mixed and unmixed solvent system indicate that the diffusive motion of ions is more in dimethyl carbonate and it decreases readily on increasing the molecules of TMS. We took the system 5 and changed the molar concentration of $LiPF_6$. Analysis of different molar concentration of salt/solvent systems indicates that the diffusive motion of ions is faster for lowest concentration of salt because cations as well as anion are more coordinated towards the dimethyl carbonate as it has more diffusion coefficient than the sulfolane. The ionic conductivities of ions with different concentration of salt also indicate that the systems with 0.52 M to 0.90 M concentration of $LiPF_6$ show more diffusive motion than the other systems having higher concentration of salt. The presented results of our simulations offer a systematic and comprehensive study of intermolecular interactions of cation-anion, anion-solvent and cation-solvent at a molecular level, which will help to understand the solvation structure and the transport properties of ions in more detail. Moreover, the appropriate electrolytes can be designed taking into account of the optimal ion diffusion for the better performance of Li-ion batteries.

■ ASSOCIATED CONTENT

Supporting Information
The forcefield parameters, additional figures and xyz coordinates of gas phase clusters are given as supporting information. “This material is available free of charge via the Internet at http://pubs.acs.org.”

■ AUTHOR INFORMATION

Corresponding Author
* E-mail: bhabani@iith.ac.in, Tel. no. +914023017051

Notes
The authors declare no competing financial interest.

■ ACKNOWLEDGEMENTS

The authors acknowledge financial support (SB/EMEQ-375/2014) for this work from Department of Science and Technology, India. Thejus R. Kartha also likes to thank MHRD, India for his PhD fellowship.

REFERENCES

(1) Wakihara, M.; Yamamoto, O. *Lithium Ion Batteries: Fundamentals and Performance*; John Wiley & Sons, 2008.

(2) Reddy, T. *Linden's Handbook of Batteries, 4th Edition*, 4 edition.; McGraw-Hill Education: New York, 2010.

(3) Kang, B.; Ceder, G. Battery Materials for Ultrafast Charging and Discharging. *Nature* **2009**, *458*, 190–193.

(4) Linden, D.; Reddy, T. B. *Handbook of Batteries*; McGraw-Hill, 2002.

(5) Beck, F.; Rüetschi, P. Rechargeable Batteries with Aqueous Electrolytes. *Electrochimica Acta* **2000**, *45*, 2467–2482.

(6) Luo, J.-Y.; Cui, W.-J.; He, P.; Xia, Y.-Y. Raising the Cycling Stability of Aqueous Lithium-Ion Batteries by Eliminating Oxygen in the Electrolyte. *Nat. Chem.* **2010**, *2*, 760–765.

(7) Kühnel, R.-S.; Reber, D.; Remhof, A.; Figi, R.; Bleiner, D.; Battaglia, C. "Water-in-Salt" Electrolytes Enable the Use of Cost-Effective Aluminum Current Collectors for Aqueous High-Voltage Batteries. *Chem. Commun.* **2016**, *52*, 10435–10438.

(8) Xu, K. Nonaqueous Liquid Electrolytes for Lithium-Based Rechargeable Batteries. *Chem. Rev.* **2004**, *104*, 4303–4418.

(9) Li, Q.; Chen, J.; Fan, L.; Kong, X.; Lu, Y. Progress in Electrolytes for Rechargeable Li-Based Batteries and Beyond. *Green Energy Environ.* **2016**, *1*, 18–42.

(10) Han, Y.-K.; Jung, J.; Cho, J.-J.; Kim, H.-J. Determination of the Oxidation Potentials of Organic Benzene Derivatives: Theory and Experiment. *Chem. Phys. Lett.* **2003**, *368*, 601–608.

(11) Wang, H.; Cui, L.-F.; Yang, Y.; Sanchez Casalongue, H.; Robinson, J. T.; Liang, Y.; Cui, Y.; Dai, H. Mn3O4−Graphene Hybrid as a High-Capacity Anode Material for Lithium Ion Batteries. *J. Am. Chem. Soc.* **2010**, *132*, 13978–13980.

(12) Xu, K.; Angell, C. A. High Anodic Stability of a New Electrolyte Solvent: Unsymmetric Noncyclic Aliphatic Sulfone. *J. Electrochem. Soc.* **1998**, *145*, L70–L72.

(13) Li, S.; Zhao, Y.; Shi, X.; Li, B.; Xu, X.; Zhao, W.; Cui, X. Effect of Sulfolane on the Performance of Lithium Bis(Oxalato)Borate-Based Electrolytes for Advanced Lithium Ion Batteries. *Electrochimica Acta* **2012**, *65*, 221–227.

(14) Wang, Y.; Xing, L.; Li, W.; Bedrov, D. Why Do Sulfone-Based Electrolytes Show Stability at High Voltages? Insight from Density Functional Theory. *J. Phys. Chem. Lett.* **2013**, *4*, 3992–3999.

(15) Abouimrane, A.; Belharouak, I.; Amine, K. Sulfone-Based Electrolytes for High-Voltage Li-Ion Batteries. *Electrochem. Commun.* **2009**, *11*, 1073–1076.

(16) Abe, T.; Fukuda, H.; Iriyama, Y.; Ogumi, Z. Solvated Li-Ion Transfer at Interface Between Graphite and Electrolyte. *J. Electrochem. Soc.* **2004**, *151*, A1120–A1123.

(17) Wu, F.; Zhou, H.; Bai, Y.; Wang, H.; Wu, C. Toward 5 V Li-Ion Batteries: Quantum Chemical Calculation and Electrochemical Characterization of Sulfone-Based High-Voltage Electrolytes. *ACS Appl. Mater. Interfaces* **2015**, *7*, 15098–15107.

(18) Xing, L.; Vatamanu, J.; Borodin, O.; Smith, G. D.; Bedrov, D. Electrode/Electrolyte Interface in Sulfolane-Based Electrolytes for Li Ion Batteries: A Molecular Dynamics Simulation Study. *J. Phys. Chem. C* **2012**, *116*, 23871–23881.

(19) Xu, K.; Angell, C. A. Sulfone-Based Electrolytes for Lithium-Ion Batteries. *J. Electrochem. Soc.* **2002**, *149*, A920–A926.

(20) Borodin, O.; Behl, W.; Jow, T. R. Oxidative Stability and Initial Decomposition Reactions of Carbonate, Sulfone, and Alkyl Phosphate-Based Electrolytes. *J. Phys. Chem. C* **2013**, *117*, 8661–8682.

(21) Abraham, M. J.; Murtola, T.; Schulz, R.; Páll, S.; Smith, J. C.; Hess, B.; Lindahl, E. GROMACS: High Performance Molecular Simulations through Multi-Level Parallelism from Laptops to Supercomputers. *SoftwareX* **2015**, *1–2*, 19–25.

(22) Martínez, L.; Andrade, R.; Birgin, E. G.; Martínez, J. M. PACKMOL: A Package for Building Initial Configurations for Molecular Dynamics Simulations. *J. Comput. Chem.* **2009**, *30*, 2157–2164.

(23) Jorgensen, W. L.; Tirado-Rives, J. The OPLS [Optimized Potentials for Liquid Simulations] Potential Functions for Proteins, Energy Minimizations for Crystals of Cyclic Peptides and Crambin. *J. Am. Chem. Soc.* **1988**, *110*, 1657–1666.

(24) M. J. Frisch, G. W. Trucks, H. B. Schlegel, G. E. Scuseria, M. A. Robb, J. R. Cheeseman, G. Scalmani, V. Barone, G. A. Petersson, H. Nakatsuji, X. Li, M. Caricato, A. Marenich, J. Bloino, B. G. Janesko, R. Gomperts, B. Mennucci, H. P. Hratchian, J. V. Ortiz, A. F. Izmaylov, J. L. Sonnenberg, D. Williams-Young, F. Ding, F. Lipparini, F. Egidi, J. Goings, B. Peng, A. Petrone, T. Henderson, D. Ranasinghe, V. G. Zakrzewski, J. Gao, N. Rega, G. Zheng, W. Liang, M. Hada, M. Ehara, K. Toyota, R. Fukuda, J. Hasegawa, M. Ishida, T. Nakajima, Y. Honda, O. Kitao, H. Nakai, T. Vreven, K. Throssell, J. A. Montgomery, Jr., J. E. Peralta, F. Ogliaro, M. Bearpark, J. J. Heyd, E. Brothers, K. N. Kudin, V. N. Staroverov, T. Keith, R. Kobayashi, J. Normand, K. Raghavachari, A. Rendell, J. C. Burant, S. S. Iyengar, J. Tomasi, M. Cossi, J. M. Millam, M. Klene, C. Adamo, R. Cammi, J. W. Ochterski, R. L. Martin, K. Morokuma, O. Farkas, J. B. Foresman, and D. J. Fox. Gaussian 09, Revision C.01. *Gaussian Inc Wallingford CT 2016*.

(25) Becke, A. D. Density-Functional Exchange-Energy Approximation with Correct Asymptotic Behavior. *Phys. Rev. A* **1988**, *38*, 3098–3100.

(26) Becke, A. D. Density- functional Thermochemistry. III. The Role of Exact Exchange. *J. Chem. Phys.* **1993**, *98*, 5648–5652.

(27) Lee, C.; Yang, W.; Parr, R. G. Development of the Colle-Salvetti Correlation-Energy Formula into a Functional of the Electron Density. *Phys. Rev. B* **1988**, *37*, 785–789.

(28) Bayly, C. I.; Cieplak, P.; Cornell, W.; Kollman, P. A. A Well-Behaved Electrostatic Potential Based Method Using Charge Restraints for Deriving Atomic Charges: The RESP Model. *J. Phys. Chem.* **1993**, *97*, 10269–10280.

(29) Case, D.; Darden, T.; Cheatham, T.; Simmerling, C.; Wang, J.; Duke, R.; Luo, R.; Crowley, M.; Walker, R.; Zhang, W.; et al. *Amber 12*.

(30) Lee, S. H.; Rasaiah, J. C. Molecular Dynamics Simulation of Ion Mobility. 2. Alkali Metal and Halide Ions Using the SPC/E Model for Water at 25 °C. *J. Phys. Chem.* **1996**, *100*, 1420–1425.

(31) Refined Potential Model for Atomistic Simulations of Ionic Liquid [Bmim][PF6]. *J. Chem. Phys.* **2007**, *127*, 114510.

(32) Muralidharan, A.; Chaudhari, M. I.; Pratt, L. R.; Rempe, S. B. Molecular Dynamics of Lithium Ion Transport in a Model Solid Electrolyte Interphase. *Sci. Rep.* **2018**, *8*, 10736.

(33) Muralidharan, A.; Chaudhari, M.; Rempe, S.; Pratt, L. R. Molecular Dynamics Simulations of Lithium Ion Transport through a Model Solid Electrolyte Interphase (SEI) Layer. *ECS Trans.* **2017**, *77*, 1155–1162.

(34) Molecular Dynamics with Coupling to an External Bath. *J. Chem. Phys.* **1984**, *81*, 3684–3690.

(35) Bussi, G.; Donadio, D.; Parrinello, M. Canonical Sampling through Velocity Rescaling. *J. Chem. Phys.* **2007**, *126*, 014101.

(36) Microcanonical Ensemble in Quantum Statistical Mechanics. *J. Math. Phys.* **1965**, *6*, 1447–1461.

(37) Brehm, M.; Kirchner, B. TRAVIS - A Free Analyzer and Visualizer for Monte Carlo and Molecular Dynamics Trajectories. *J. Chem. Inf. Model.* **2011**, *51*, 2007–2023.

(38) Moosavi, M.; Motahari, A.; Vahid, A.; Akbar, V.; Rostami, A. A.; Omrani, A. Densities, Viscosities, and Refractive Indices of Dimethyl Carbonate + 1-Hexanol/1-Octanol Binary Mixtures at Different Temperatures. *J. Chem. Eng. Data* **2016**, *61*, 1981–1991.

(39) Steele, W. V.; Chirico, R. D.; Knipmeyer, S. E.; Nguyen, A. Vapor Pressure, Heat Capacity, and Density along the Saturation Line, Measurements for Cyclohexanol, 2-Cyclohexen-1-One, 1,2-Dichloropropane, 1,4-Di-Tert-Butylbenzene, (±)-2-

Ethylhexanoic Acid, 2-(Methylamino)Ethanol, Perfluoro-n-Heptane, and Sulfolane. *J. Chem. Eng. Data* **1997**, *42*, 1021–1036.

(40) Eilmes, A.; Kubisiak, P. Quantum-Chemical and Molecular Dynamics Study of M+[TOTO]− (M = Li, Na, K) Ionic Liquids. *J. Phys. Chem. B* **2013**, *117*, 12583–12592.

(41) Borodin, O.; Smith, G. D. Quantum Chemistry and Molecular Dynamics Simulation Study of Dimethyl Carbonate: Ethylene Carbonate Electrolytes Doped with LiPF6. *J. Phys. Chem. B* **2009**, *113*, 1763–1776.

(42) Chandler, D. *Introduction to Modern Statistical Mechanics*, 1 edition.; Oxford University Press: New York, 1987.

(43) Del Pópolo, M. G.; Voth, G. A. On the Structure and Dynamics of Ionic Liquids. *J. Phys. Chem. B* **2004**, *108*, 1744–1752.

(44) Islam, M. A. Einstein–Smoluchowski Diffusion Equation: A Discussion. *Phys. Scr.* **2004**, *70*, 120.

(45) *Theory of Simple Liquids*; Elsevier, 2006.

(46) An Energy Dispersive X-Ray Scattering and Molecular Dynamics Study of Liquid Dimethyl Carbonate. *J. Chem. Phys.* **2009**, *131*, 244503.

(47) Hayamizu, K.; Aihara, Y.; Arai, S.; Martinez, C. G. Pulse-Gradient Spin-Echo 1H, 7Li, and 19F NMR Diffusion and Ionic Conductivity Measurements of 14 Organic Electrolytes Containing LiN(SO2CF3)2. *J. Phys. Chem. B* **1999**, *103*, 519–524.

(48) Lee, S.-Y.; Ueno, K.; Angell, C. A. Lithium Salt Solutions in Mixed Sulfone and Sulfone-Carbonate Solvents: A Walden Plot Analysis of the Maximally Conductive Compositions. *J. Phys. Chem. C* **2012**, *116*, 23915–23920.

(49) Reddy, T. D. N.; Mallik, B. S. Protic Ammonium Carboxylate Ionic Liquids: Insight into Structure, Dynamics and Thermophysical Properties by Alkyl Group Functionalization. *Phys. Chem. Chem. Phys.* **2017**, *19*, 10358–10370.

(50) Hayamizu, K. Temperature Dependence of Self-Diffusion Coefficients of Ions and Solvents in Ethylene Carbonate, Propylene Carbonate, and Diethyl Carbonate Single Solutions and Ethylene Carbonate + Diethyl Carbonate Binary Solutions of LiPF6 Studied by NMR. *J. Chem. Eng. Data* **2012**, *57*, 2012–2017.

(51) Yang, S.; Yan, B.; Wu, J.; Lu, L.; Zeng, K. Temperature-Dependent Lithium-Ion Diffusion and Activation Energy of $Li_{1.2}Co_{0.13}Ni_{0.13}Mn_{0.54}O_2$ Thin-Film Cathode at Nanoscale by Using Electrochemical Strain Microscopy. *ACS Appl. Mater. Interfaces* **2017**, *9*, 13999–14005.

Table 1. Number of ion pairs/molecules and corresponding density at 330 K of investigated system with fixed no of $LiPF_6$ and variation of no of DMC and TMS molecules.

System	$LiPF_6$	DMC	TMS	Density [gm cm^{-3}]
1	30	300	0	1.14
2	30	0	300	1.27
3	30	200	100	1.19
4	30	150	150	1.22
5	30	100	200	1.24

Table 2. Number of ion pairs/molecules, concentration and density at 330 K of corresponding systems containing various concentration of $LiPF_6$ with fixed DMC/TMS molar ratio of 1:2.

System	$LiPF_6$	DMC	TMS	Concentration[M]	Density [gm cm^{-3}]
5a	15	100	200	0.545	1.20
5b	20	100	200	0.727	1.21
5c	25	100	200	0.90	1.22
5d	35	100	200	1.27	1.25
5e	40	100	200	1.45	1.26

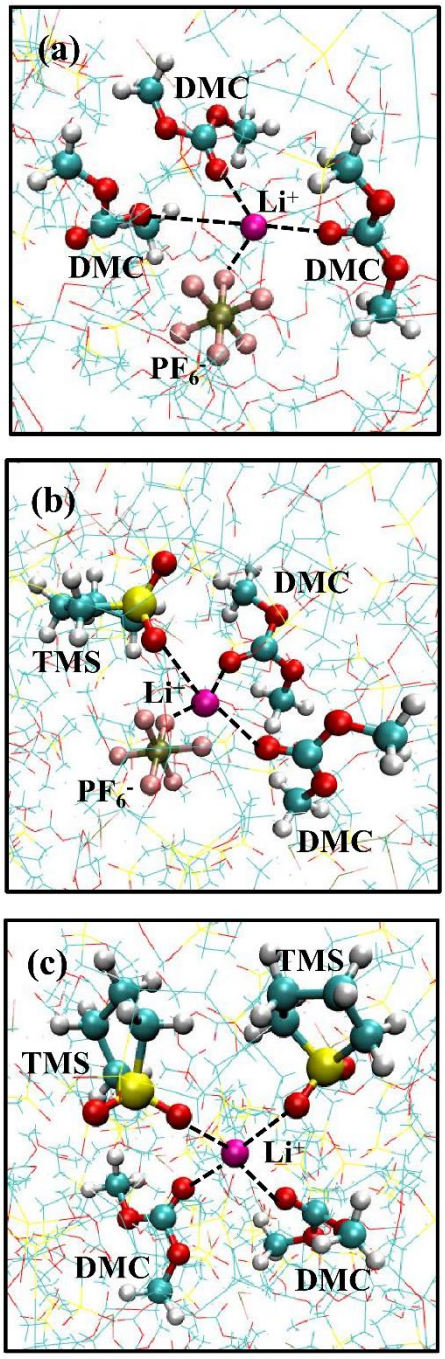

Figure 1. Snapshots of (a) $Li(DMC)_3PF_6$ from system 3 which contains DMC:TMS::2:1 (b) $Li(TMS)(DMC)_2PF_6$ from system 4 which contains DMC:TMS::1:1 (c) $[Li(TMS)_2(DMC)_2]^+$ from system 5 which contains DMC:TMS::1:2, after NVE simulations.

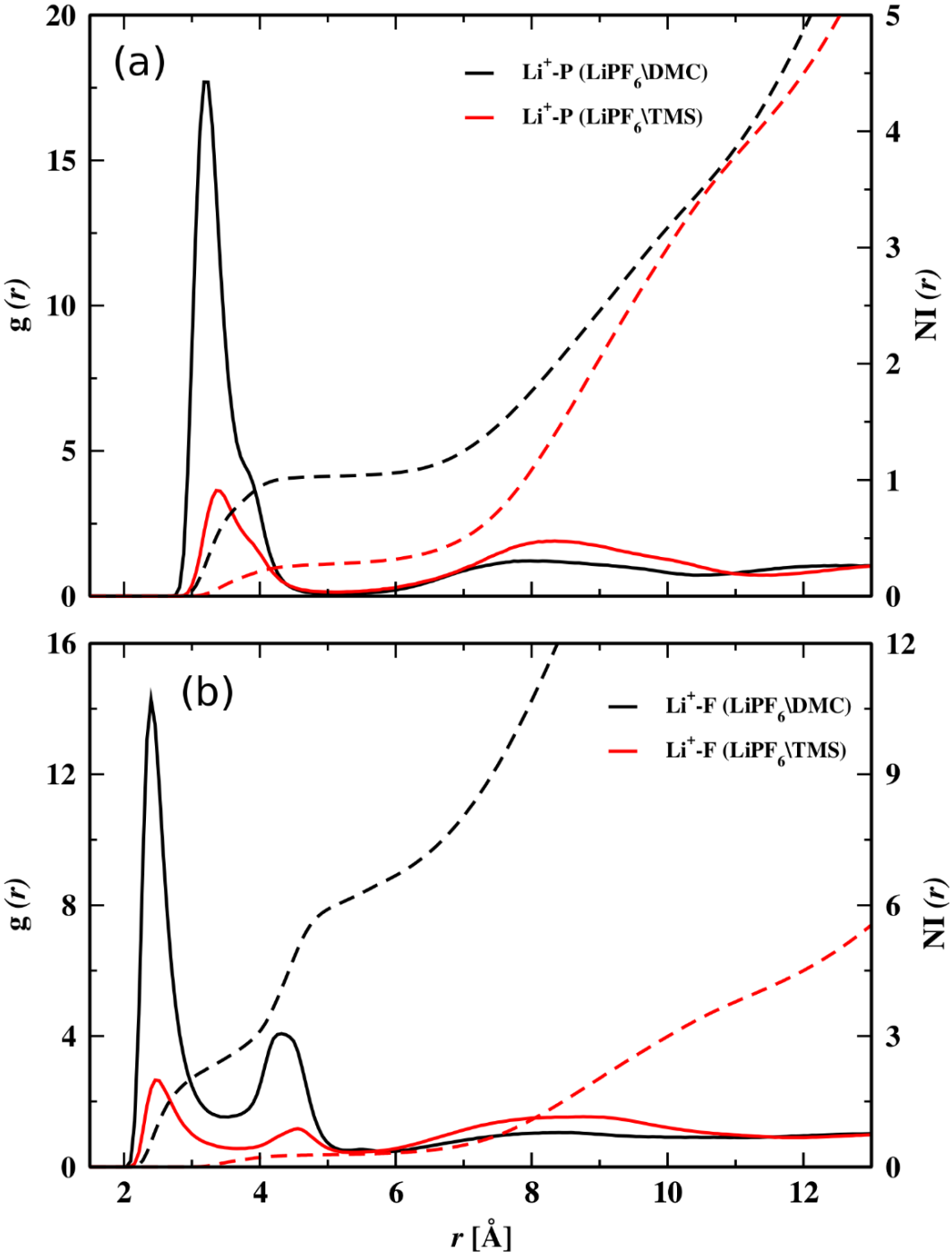

Figure 2. Radial distribution functions (solid lines) and corresponding number integrals (dashed lines): The panels (a) and (b) represent the correlation of Li^+ with phosphorus and fluorine atoms of anion, respectively, in DMC and TMS.

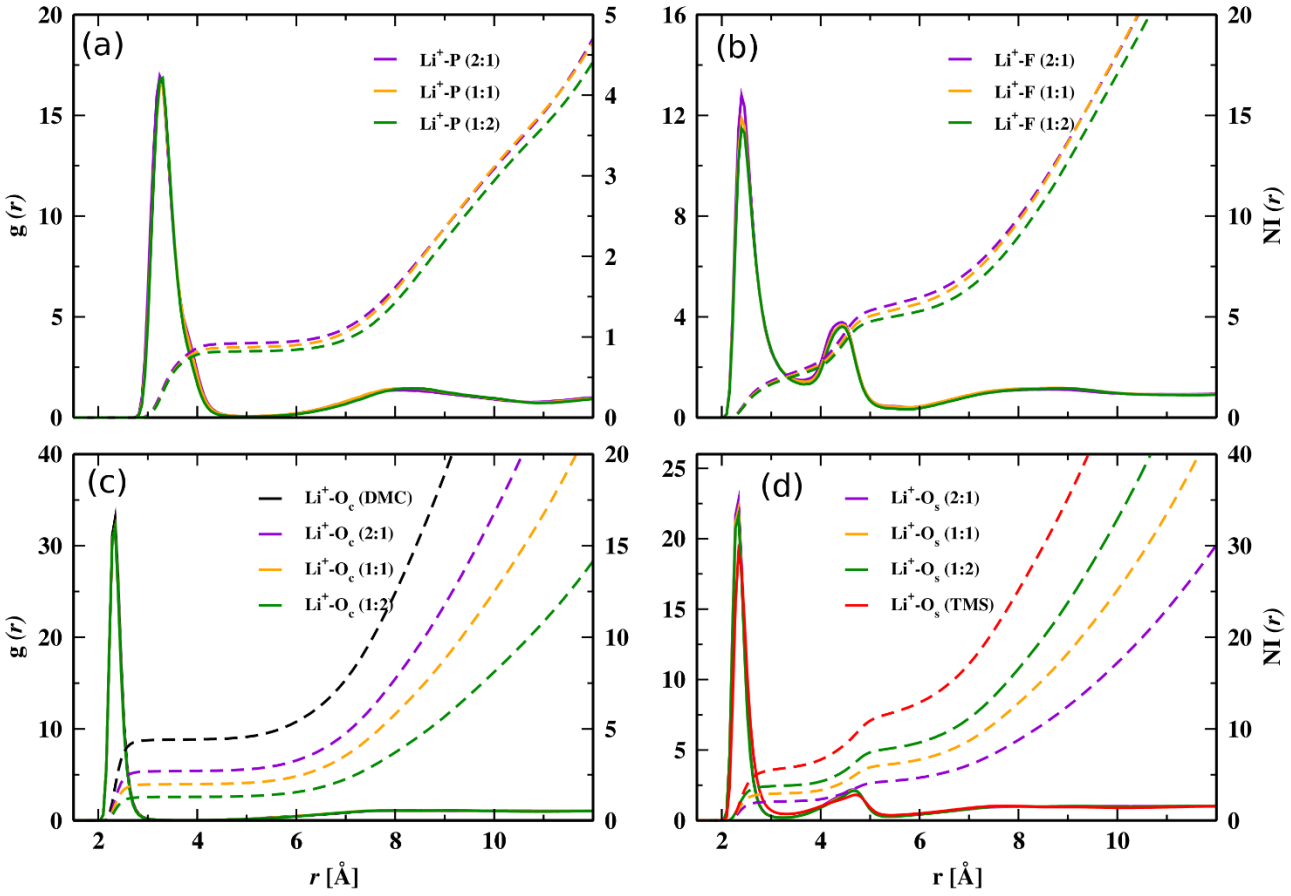

Figure 3. Radial distribution functions (solid lines) and corresponding number integrals (dashed lines); The panels (a) and (b) represent the correlation of Li^+ with phosphorus and fluorine atoms of anion, respectively, in the mixtures of DMC and TMS. The panel (c) represents the correlation of Li^+ with carbonyl oxygen atom of DMC in pure as well as mixtures. The panel (d) depicts the correlation of Li^+ with oxygen atoms of TMS in pure and mixture of solvents.

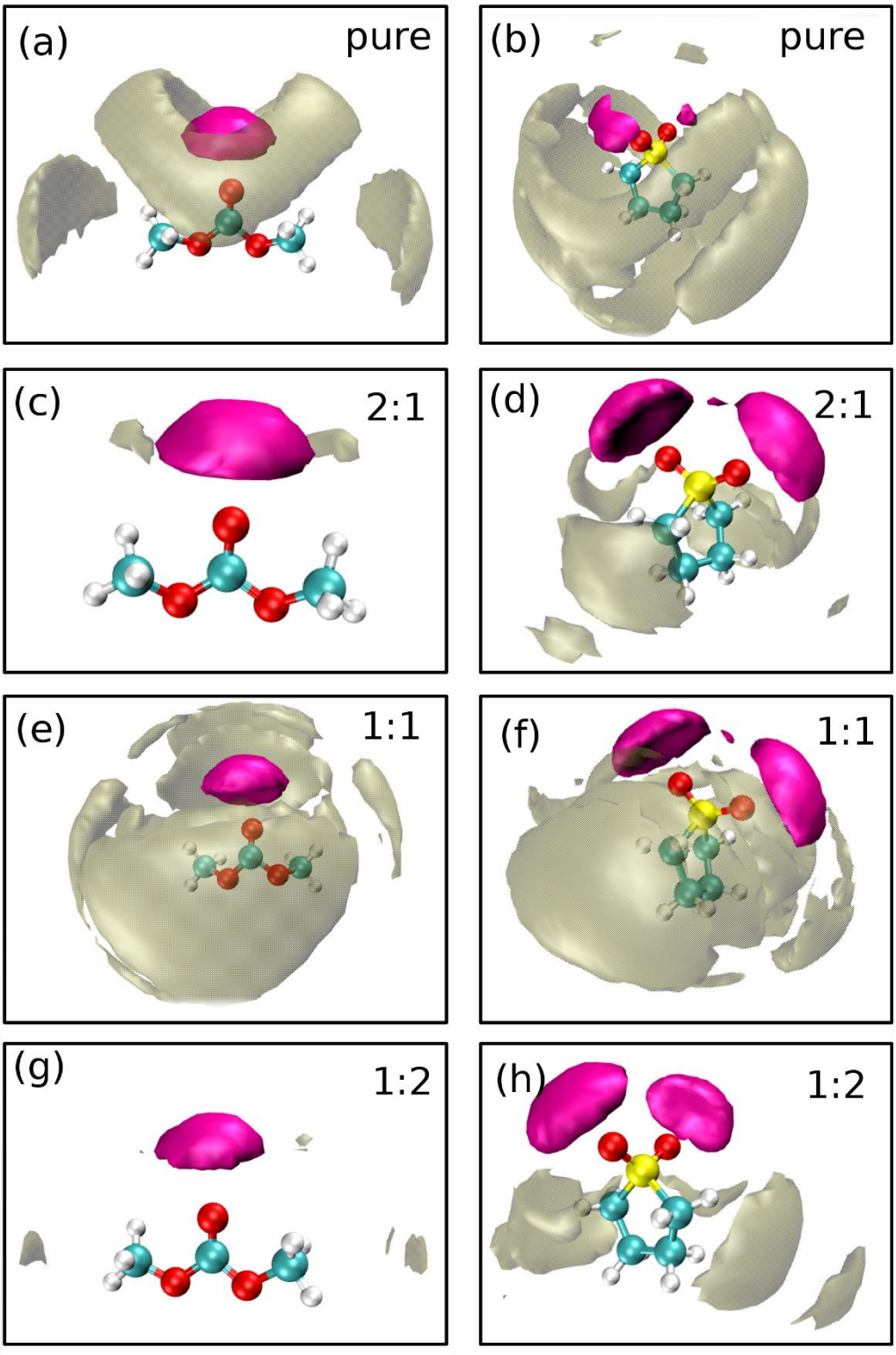

Figure 4. Spatial distribution functions of the salt-solvent interaction in pure and mixtures. Cation and anion are represented by magenta and tan isosurfaces, respectively, within isovalue of 0.2(cation) and 1(anion) particles/nm^3.

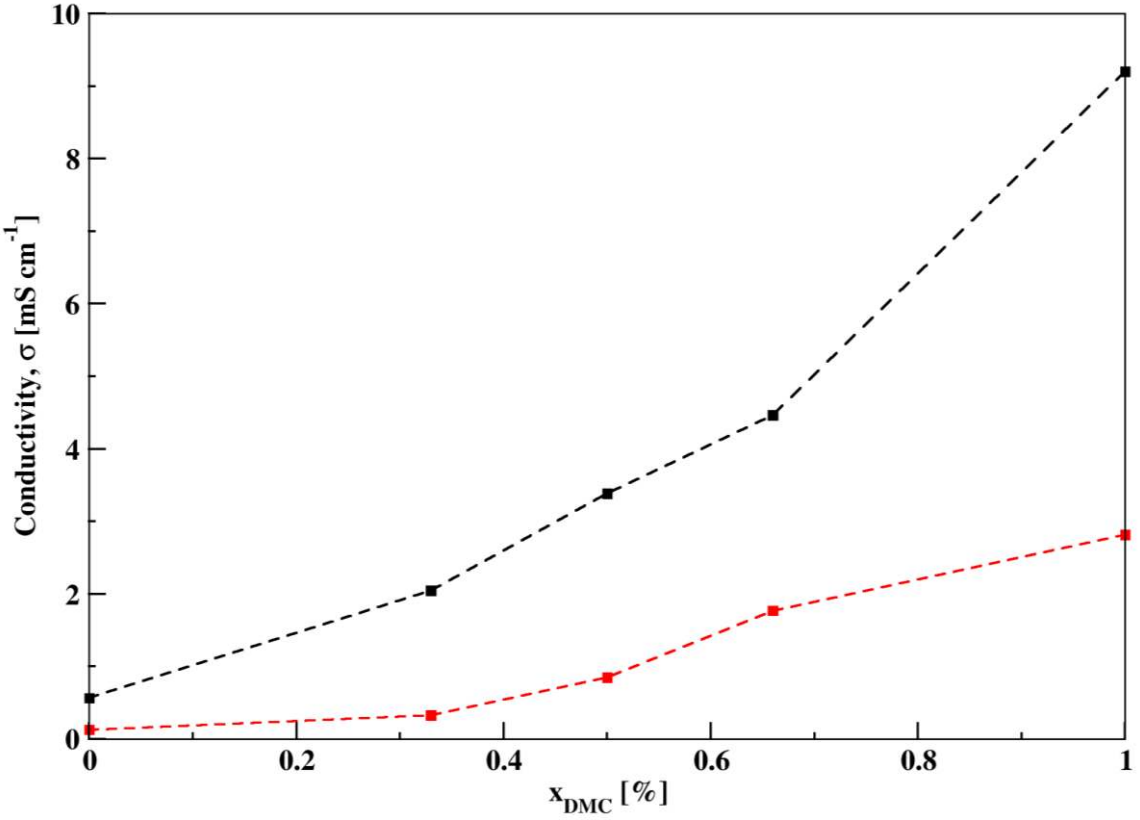

Figure 5. Ionic conductivity (inset figure) of $LiPF_6$ on increasing the mole fraction of DMC in mixture. The black line shows ionic conductivity calculated from self-diffusion coefficients of Li^+ and PF_6^- ions. The red line shows correlated conductivity calculated from mutually-correlated motion of ions.

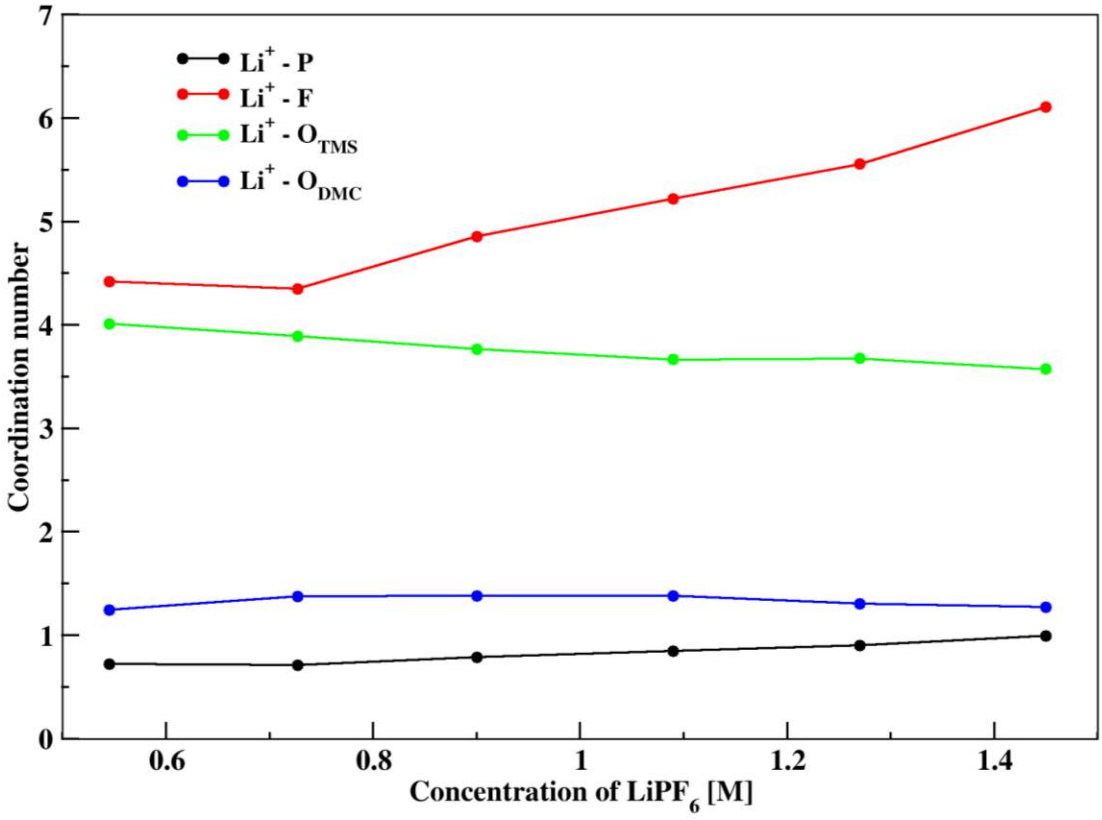

Figure 6. Changing coordination number values with change in concentration, for different interaction pairs.

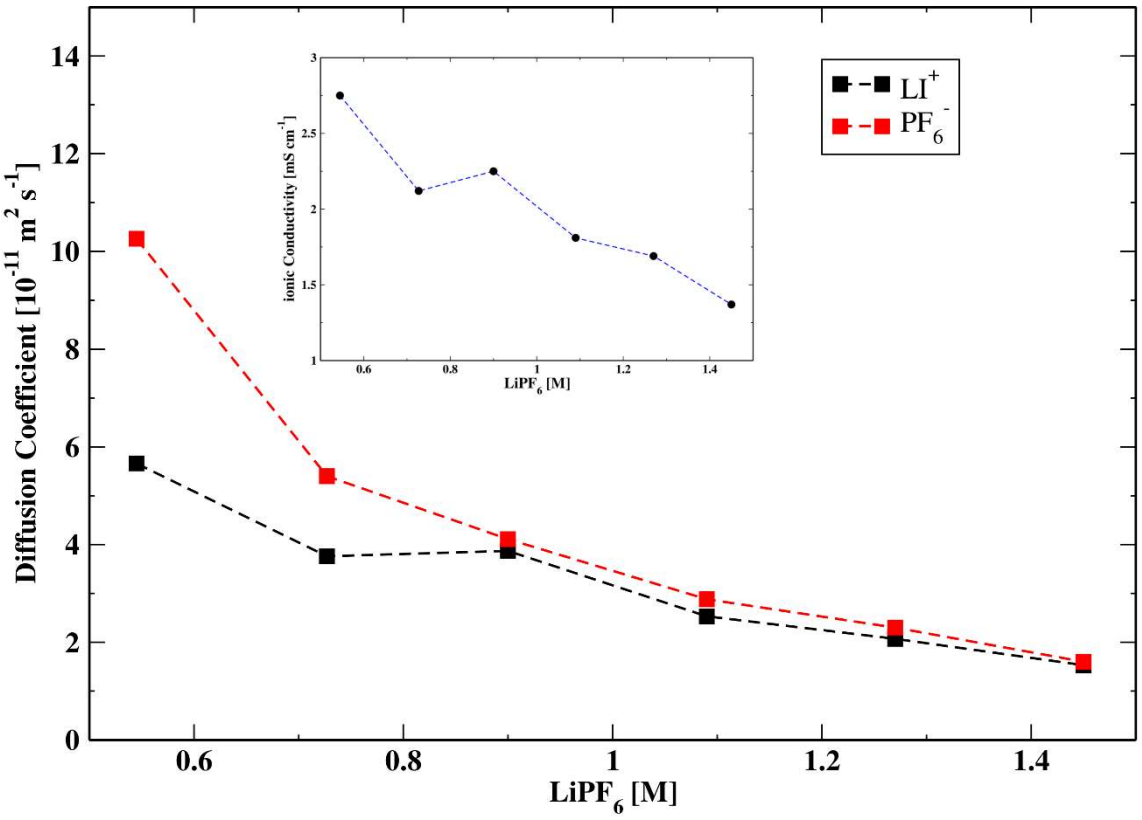

Figure 7. Illustrates the diffusion coefficients of cation as well as anion and ionic conductivity of $LiPF_6$ on changing the salt concentration in system 5.

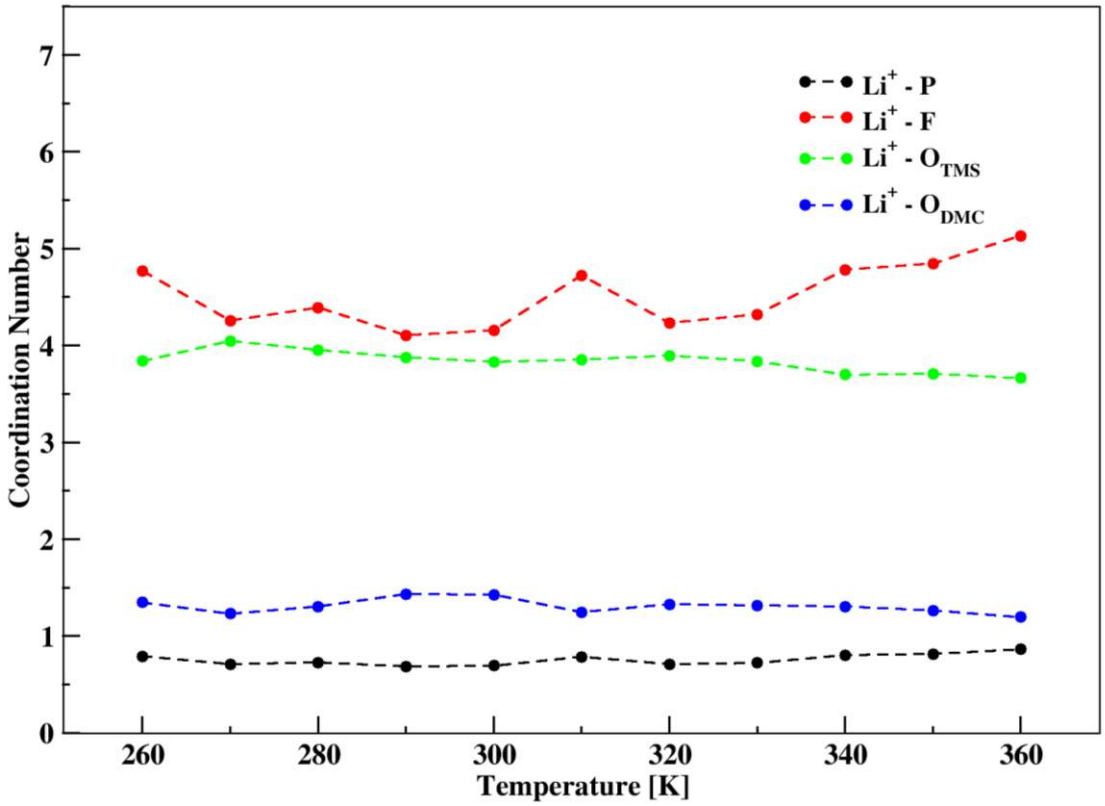

Figure 8. Change in coordination numbers with respect to change in temperature.

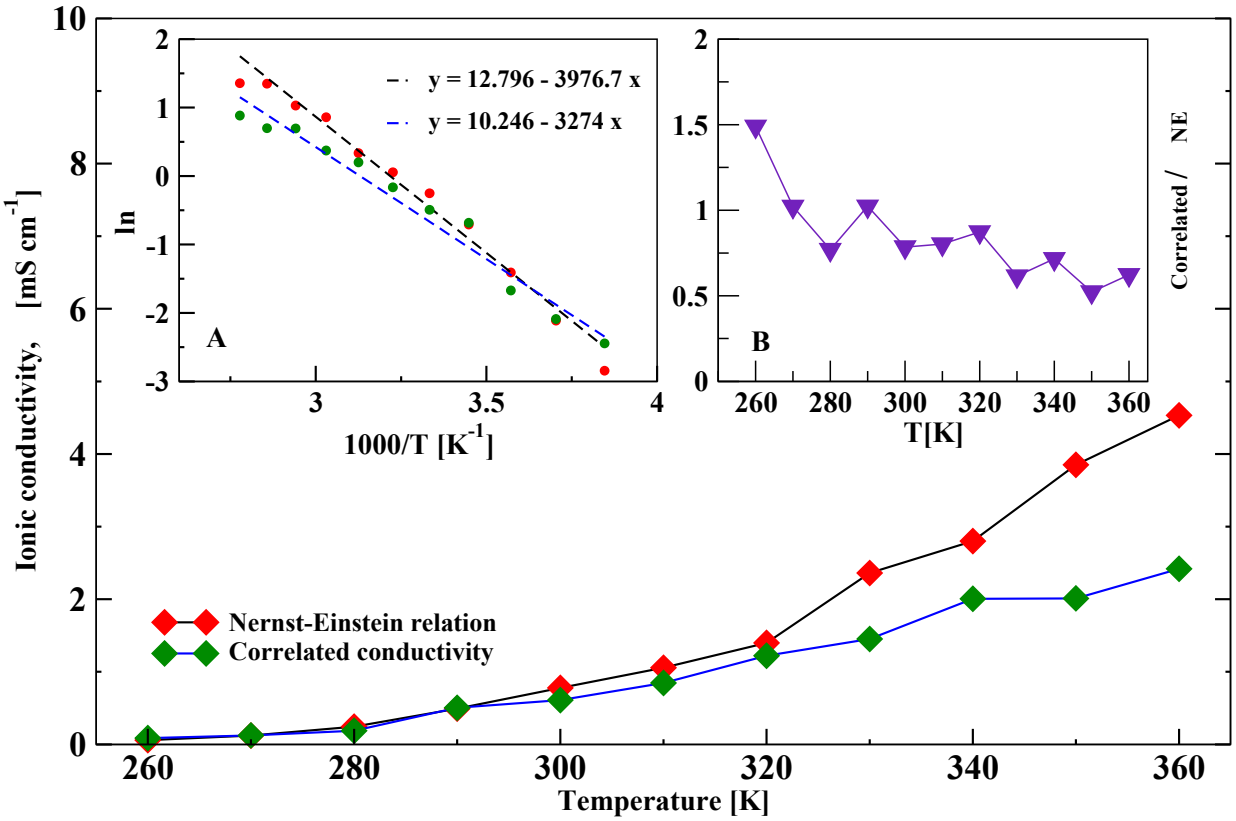

Figure 9. Temperature dependent ionic conductivity. Inset figure (A) represents Arrhenius plot of the temperature dependency of ionic conductivity. The equations of linear fit are provided, and they have the correlation coefficients 0.989 (black line) and 0.984 (blue line). Inset figure (B) depicts variation of degree of ionicity (ratio of correlated conductivity and conductivity obtained from Nernst-Einstein relation) with temperature.

TOC Graphics